ECS Journal of Solid State
Science and Technology

The Electrochemical Society
Advancing solid state & electrochemical science & technology

OPEN ACCESS

Atomic Layer Deposition and Properties of HfO_2-Al_2O_3 Nanolaminates

To cite this article: Kaupo Kukli *et al* 2018 *ECS J. Solid State Sci. Technol.* **7** P501

View the article online for updates and enhancements.

This content was downloaded from IP address 157.88.20.207 on 08/01/2021 at 12:10

Atomic Layer Deposition and Properties of HfO_2-Al_2O_3 Nanolaminates

Kaupo Kukli,[1,2,z] Marianna Kemell,[1] Helena Castán,[3] Salvador Dueñas,[3] Helina Seemen,[2] Mihkel Rähn,[2] Joosep Link,[4] Raivo Stern,[4] Mikko Ritala,[1,*] and Markku Leskelä[1]

[1]*Department of Chemistry, University of Helsinki, FI-00014 Helsinki, Finland*
[2]*Institute of Physics, University of Tartu, 50411 Tartu, Estonia*
[3]*Department of Electronics, University of Valladolid, 47011 Valladolid, Spain*
[4]*National Institute of Chemical Physics and Biophysics, 12618 Tallinn, Estonia*

Nanocrystalline HfO_2:Al_2O_3 mixture films and nanolaminates were grown by atomic layer deposition at 350°C from metal chloride precursors and water. Formation of metastable HfO_2 polymorphs versus monoclinic phase was affected by the relative amount and thickness of constituent oxide layers. The films exhibited saturative magnetization and charge polarization in externally applied fields at room temperature. The films also demonstrated resistive switching behavior with considerable window between low and high resistance states.
© The Author(s) 2018. Published by ECS. This is an open access article distributed under the terms of the Creative Commons Attribution 4.0 License (CC BY, http://creativecommons.org/licenses/by/4.0/), which permits unrestricted reuse of the work in any medium, provided the original work is properly cited. [DOI: 10.1149/2.0261809jss]

Manuscript submitted June 29, 2018; revised manuscript received August 21, 2018. Published September 6, 2018.

Composites and multilayers of chemically distinct metal oxides are of continuous interest as materials tailoring useful electronic, mechanical and structural properties of their constituents which increase their suitability to many applications. Herewith hafnium-aluminum-oxide thin films have been studied as insulating dielectrics potentially suited to application as gate dielectric materials in MOSFET structures with Si,[1–5] $Si_{0.7}Ge_{0.3}$,[6] $In_xGa_{1-x}As$,[7,8] or InP,[9,10] as well as memory capacitor dielectrics in three-dimensional DRAM structures.[11] For flash memory cell structures, different charge trapping materials HfO_2, Hf-Al-O and Al_2O_3 have been compared in metal-oxide-semiconductor capacitors with fixed Al_2O_3 tunneling and blocking layers and Pd-electrode.[12] HfO_2-Al_2O_3 mixtures have been studied as buffer layers in Pt/$SrBi_2Ta_2O_9$/$(HfO_2)_x(Al_2O_3)_{1-x}$ ferroelectric RAM cells.[13] Al_2O_3/HfO_2/Al_2O_3 trilayer structures have exhibited promising switching resistance memory behavior.[14] Properties of HfO_2–Al_2O_3 nanolaminates, as well as mixtures, have also been investigated in more general terms such as chemical and phase composition, though mainly intended for MIM or CMOS based DRAM applications,[2,15] or as non-volatile resistive switching memory (memristor) materials.[16–18] Al-doping in HfO_2 has been found useful when modifying defect densities and stoichiometry in dielectrics for MOS-devices.[19,20]

Cubic and tetragonal polymorphs of HfO_2 knowingly possess higher dielectric permittivity compared to that of monoclinic phase,[21] and have thus been attractive for applications in capacitive memory devices and electronic switches.[22] The orthorhombic phase may also be considered as an interesting one in terms of electrical charge polarization, since, due to its noncentrosymmetric lattice, it could be responsible for the ability of the material to nonlinearly and saturatively polarize in external electric field. Such films can demonstrate remnant polarization and coercivity, forming polarization loops with marked hystereses as characteristic of ferroelectric materials. Corresponding behavior in HfO_2 films doped with Al has been reported earlier.[23,24] Stabilization of metastable (incl. orthorhombic) HfO_2 films grown by atomic layer deposition using various dopants including Al_2O_3,[25] and their ferroelectric-like behavior[26] have already been described in some papers to date. At the same time, magnetization behavior in the same films has not yet been studied.

In general, layered transition metal oxides have gained attention as materials able to exhibit both magnetoelectric and resistive switching behavior.[27] Resistive switching, ferromagnetic and ferroelectric polarization have simultaneously been registered and investigated in rather complex stacked compounds, such as $Bi_{0.8}Pr_{0.2}Fe_{0.95}Mn_{0.05}O_3$/$Bi_{3.96}Gd_{0.04}Ti_{2.95}W_{0.05}O_{12}$/Pt(111)/Ti/$SiO_2$/Si(100).[28] Defects, in particular oxygen vacancies, have presumably been responsible for the switching behavior, concurrent electrical modulation and the following electrical field coupling with magnetization of the same material. Resistive switching possibly affecting electrical control of ferromagnetism in Ag/HfO_2/Nb:$SrTiO_3$/Ag stacks has been reported.[29] Coexistence of electric field controlled ferromagnetism and resistive switching in transition metal oxide films has been recorded at room temperature earlier in TiO_2 based stacks.[30] Switching currents were also measured in atomic layer deposited, presumably ferroelectric, $Hf_{0.5}Zr_{0.5}O_2$ thin films.[31] Therefore, simultaneous evaluation of magnetization behavior, electrical polarization and switching resistivity effects in the same solid films appear justified. Recently, a study on ZrO_2-Al_2O_3 doped films and nanolaminates was published, describing the electric and magnetic behavior of these materials.[32] Nonlinear saturative magnetization was achieved in the laminated structure, referring to ferromagnetic-like behavior. At the same time, electric charge polarization in ZrO_2-Al_2O_3 stacked layers was markedly affected by the interfacial polarization, possibly with weak ferroelectric component contributing to the polarization-field curves measured. The electronic leakage currents in these laminates and doped films were considerable, although allowing definitive switching between high and low resistance states. The switching was positively influenced by the inclusion of Al_2O_3 dopant layers.[32]

Apart from scarce studies on HfO_2-Al_2O_3 multilayers produced by physical methods such as sputtering,[2] HfO_2-Al_2O_3 films have mainly and most feasibly been processed by atomic layer deposition (ALD). HfO_2-Al_2O_3 mixtures and multilayer films have been synthesized by ALD from $Al(CH_3)_3$, $Hf[N(CH_3)(C_2H_5)]_4$ and H_2O;[7,9,12,14,33] $Al(CH_3)_3$, $Hf[N(CH_3)_2]_4$ and H_2O;[3,4] $Al(CH_3)_3$, $Hf[N(CH_3)_2]_4$ and O_2 plasma;[34] $Al(CH_3)_3$, $Hf[N(CH_3)(C_2H_5)]_4$ and O_2 plasma;[5] $Al(CH_3)_3$, $HfCl_4$ and H_2O.[6,15] At least one of the metal precursors in those experiments were aluminum alkyl or hafnium alkylamide compounds, i.e. precursors which knowingly provide growth of thin films uniformly over arbitrarily shaped substrates. On the other hand, the growth experiments are then limited to temperatures 200–250°C or below, because these precursors are prone to thermal decomposition. For instance, Al_2O_3-HfO_2 nanolaminates were grown by ALD from $Al(CH_3)_3$, $Hf[N(CH_3)_2]_4$ and H_2O at 225°C,[3,4] and from $Al(CH_3)_3$, $Hf[N(CH_3)(C_2H_5)]_4$ and O_2 plasma at 150°C[5] with post-deposition annealing at 350 and 850°C, respectively, in order to improve the film structure and reduce the defect densities.

In the present study, HfO_2-Al_2O_3 nanolaminates were grown by ALD in order to investigate the phase composition of HfO_2 layers grown to variable thicknesses between the intermediate Al_2O_3 constraint layers. The experiments were carried out using thermally stable

*Electrochemical Society Member.
[z]E-mail: kaupo.kukli@helsinki.fi; kaupo.kukli@ut.ee

Table I. HfO_2-Al_2O_3 mixture and nanolaminate films grown using cycle sequences indicated and listed in the order of ascending total HfO_2 cycle numbers in relation to those of Al_2O_3. Film thicknesses, d, and Hf:Al cation ratios were determined by EDX.

HfO_2:Al_2O_3 cycle ratio	growth cycle sequences	d,nm	Hf:Al
(15:4)	$31 \times [15 \times HfO_2 + 4 \times Al_2O_3] + 15 \times HfO_2$	41	1.8
(15:3)	$33 \times [15 \times HfO_2 + 3 \times Al_2O_3] + 15 \times HfO_2$	34	2.7
(15:2)	$34 \times [15 \times HfO_2 + 2 \times Al_2O_3] + 15 \times HfO_2$	32	2.8
(50:5)	$11 \times [50 \times HfO_2 + 5 \times Al_2O_3] + 50 \times HfO_2$	37	4.4
(15:1)	$35 \times [15 \times HfO_2 + 1 \times Al_2O_3] + 15 \times HfO_2$	33	3.3
(150:10)	$4 \times [150 \times HfO_2 + 10 \times Al_2O_3] + 150 \times HfO_2$	44	3.5
(170:10)	$4 \times [170 \times HfO_2 + 10 \times Al_2O_3] + 170 \times HfO_2$	48	6.4
(100:5)	$5 \times [100 \times HfO_2 + 5 \times Al_2O_3] + 100 \times HfO_2$	41	4.2
(120:6)	$5 \times [120 \times HfO_2 + 6 \times Al_2O_3] + 120 \times HfO_2$	24	4.5
(200:10)	$3 \times [200 \times HfO_2 + 10 \times Al_2O_3] + 200 \times HfO_2$	48	5.4
(150:5)	$3 \times [150 \times HfO_2 + 5 \times Al_2O_3] + 150 \times HfO_2$	38	5.7
(100:2)	$6 \times [100 \times HfO_2 + 2 \times Al_2O_3] + 100 \times HfO_2$	24	2.3
(300:5)	$2 \times [300 \times HfO_2 + 5 \times Al_2O_3] + 300 \times HfO_2$	19	1.9
(100:1)	$6 \times [100 \times HfO_2 + 1 \times Al_2O_3] + 100 \times HfO_2$	43	-
HfO_2	$700 \times HfO_2$, reference film	42	

metal chloride precursors, i.e. $AlCl_3$ and $HfCl_4$. The deposition temperature, 350°C, was chosen higher than that most commonly used, 300°C, in chloride-based ALD process, to enhance ordering and provide well-defined crystal growth in the as-deposited HfO_2 films.[35] At the same time, the temperature chosen was sufficiently low to enable reasonably high nucleation density followed by development of continuous solid material layers beginning from the earliest stages of the growth process, since even higher deposition temperatures might reduce the nucleation density, increase the grain size and cause significant structural defects and voids.[36] After the growth experiments, the films were electrically evaluated in their as-deposited states without further heat-treatments. The films were also characterized in terms of electrical charge and magnetic polarization in external fields.

Experimental

The films were grown in a commercial flow-type hot-wall reactor F120 (ASM Microchemistry, Ltd.)[37] from $HfCl_4$ (99.9%, Strem), $AlCl_3$ (99%, Acros Organics) and H_2O. The growth temperature was held at 350°C. $HfCl_4$ and $AlCl_3$ were evaporated at 170 and 95°C, respectively from open boats inside the reactor, and transported to the substrates by the N_2 flow. The cycle times used were 0.5–0.5–0.5–0.5 s, denoting the sequence metal precursor pulse–purge–water pulse–purge. The substrates were rectangular pieces cut out of undoped Si(100) with maximum edge length of 5 cm, covered with a 1.5–2.0 nm thick wet-chemically-grown SiO_2. In addition, also conducting electrode substrates were used for the deposition of HfO_2, based on (100) silicon with a resistivity of 0.014–0.020 $\Omega \cdot$cm, i.e., boron-doped to concentrations up to $5 \times 10^{18} - 1 \times 10^{19}/cm^3$, and coated with 10 nm thick chemical vapor deposited titanium nitride layer. The films were grown to thicknesses ranging from ca. 5 to 100 nm, i.e. also relatively thicker than those subjected to electrical measurements, in order to make the structural and compositional measurements more convenient. The Al to Hf content was varied by changing the ratio of the subsequent Al_2O_3 and HfO_2 deposition cycles. The number of subsequent Al_2O_3 and HfO_2 deposition cycles was varied separately in order to change the thicknesses of constituent metal oxide layers. In this way, films of different structures were deposited, ranging from HfO_2 mixed with low amounts of Al_2O_3 to Al_2O_3-HfO_2 nanolaminates. The growth cycle sequences applied for the different samples are given in Table I.

PANalytical X'pert Pro MPD diffractometer was used to measure grazing incidence X-ray diffraction patterns with the incident beam angle of 1°. Energy dispersive X-ray spectrometry (EDX) was applied for the measurements of the hafnium to aluminum cation ratio, and also for the estimation of the film thicknesses, using a Hitachi S-4800 scanning electron microscope (SEM) equipped with an Oxford INCA 350 EDX spectrometer. The EDX spectra were measured at 5 keV. The beam current and spectrometer gain were determined from a calibration measurement under the same beam conditions. The film thicknesses and ratios of the different elements were calculated from the k ratios of Hf Mα, and Al Kα X-ray lines measured with the calibrated beam. These calculations were done with a GMRFILM program.[38] The thicknesses were calculated using a film density of 9 g/cm^3. The selected nanolaminates on Si substrate were investigated by scanning electron microscopy (SEM) using FEI Helios Nanolab 600 DualBeam microscope equipped with focused ion beam (FIB) module and Omniprobe model 100.7 in-situ nanomanipulator. High-resolution transmission electron microscopy (HRTEM) studies for the characterization of the cross-sections of the nanolaminate structures were carried out using FEI Titan Themis 200 instrument with a field emission gun operated at 200 kV.

Magnetic measurements on selected samples were performed using vibrating sample magnetometer (VSM) option of the Physical Property Measurement System (PPMS) 14 T (Quantum Design), with the magnetic field parallel to the film surface. For electrical measurements, Al/Ti/HfO_2-Al_2O_3/TiN/Si/Al capacitor stacks were constructed with the effective capacitor area of 0.204 mm^2. Double-layer 110 nm/50 nm thick Al/Ti dot electrodes were evaporated through a shadow mask on the top HfO_2 layers by electron beam evaporation, the Ti layer being in direct contact to the top HfO_2. Backside ohmic contact was provided by evaporating 100–120 nm thick Al layer on HF-etched Si. Electrical measurements were done by means of an Agilent DXO-X 3104 digital oscilloscope with a built-in wave generator. The standard Sawyer-Tower experiment was carried out by applying a periodic triangular-shaped stimulus and recording the voltage loops data from the oscilloscope. Charge values were obtained from the sensed voltage across a stated capacitance.

Results and Discussion

Film structure.—The HfO_2-based films grown in the present study, except those mixed with Al_2O_3 in large amounts, tended to crystallize in the as-deposited state, as expected. The multilayered films consisted of distinct Al_2O_3 and HfO_2 layers, as revealed by HRTEM images (Figure 1). One could also see that the very first HfO_2 layers, closest to the Si substrate, occurred more disordered, while the crystal growth inside the hafnium oxide layers became more prominent toward the surface of the nanolaminate film.

The HfO_2 films grown without mixing with Al_2O_3, i.e. the reference HfO_2 films, were polycrystalline, as recognized by X-ray diffraction studies (Fig. 2), consisting of the stable monoclinic phase and metastable phases. The metastable phases of HfO_2 to be considered are cubic, tetragonal and orthorhombic polymorphs. Almost all the reflection peaks in the GIXRD pattern of the reference hafnium oxide can be attributed to the monoclinic HfO_2. There is only one strong

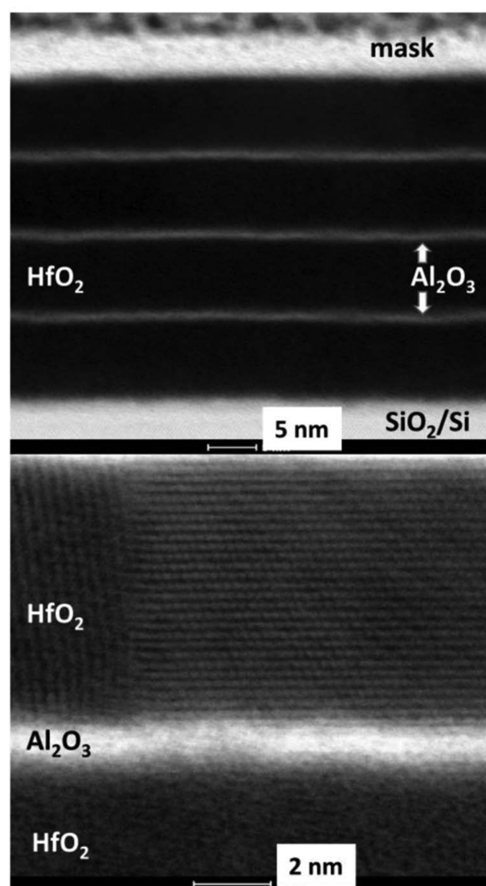

Figure 1. HRTEM cross-section images of a nanolaminate grown using HfO_2:Al_2O_3 cycle ratio of (200:10). The lower panel depicts an image taken from the top HfO_2 layer.

peak, apparent at 30.3°, which does belong to some metastable phase and not to the monoclinic one. It is, however, to be mentioned, that many reflections originating from the different phases locate close to each other. Thus, it is rather complicated to unambiguosly separate the monoclinic phase from the metastable ones at diffraction angles higher than 33–35°. It is also complicated to unambiguously distinguish between the orthorhombic, cubic, and tetragonal phases because even the strongest characteristic peak at 30.3° may shift due to internal stresses and be too wide, as characteristic of nanocrystalline materials, for the precise phase determination.

Also the nanolaminate films containing HfO_2 layers grown to relatively large nominal thicknesses (300 cycles, nominally ca. 15 nm) between very thin (e.g. 5 cycles) intermediate Al_2O_3 layers, can be regarded as multiphase materials, but with strenghtened contribution from the metastable polymorphs, decided mainly on the basis of the relative intensity of the peak at 30.3°.

It is to be noted that the aluminum to hafnium cation ratios as measured and revealed in the Table I, tend to be higher that those expected after considering the nominal ratios of Al_2O_3 and HfO_2 growth cycles. This can, partially, become explained by difficulties in accurate determination of the content of metals in the films. Under the measurement conditions used here, it is more complicated for hafnium than for aluminum due to the proximity of the Hf Mα and Si Kα lines which my make the Hf content appear higher than it actually is. On the other hand, the relative content of aluminum may also increase through surface reactions between adsorbing $AlCl_3$ and underlying HfO_2, resulting in conversion of some HfO_2 to the thermodynamically more stable Al_2O_3, similarly to the process considered earlier in the case of ZrO_2-Al_2O_3 nanolaminates grown from $ZrCl_4$, $AlCl_3$ and H_2O.[39]

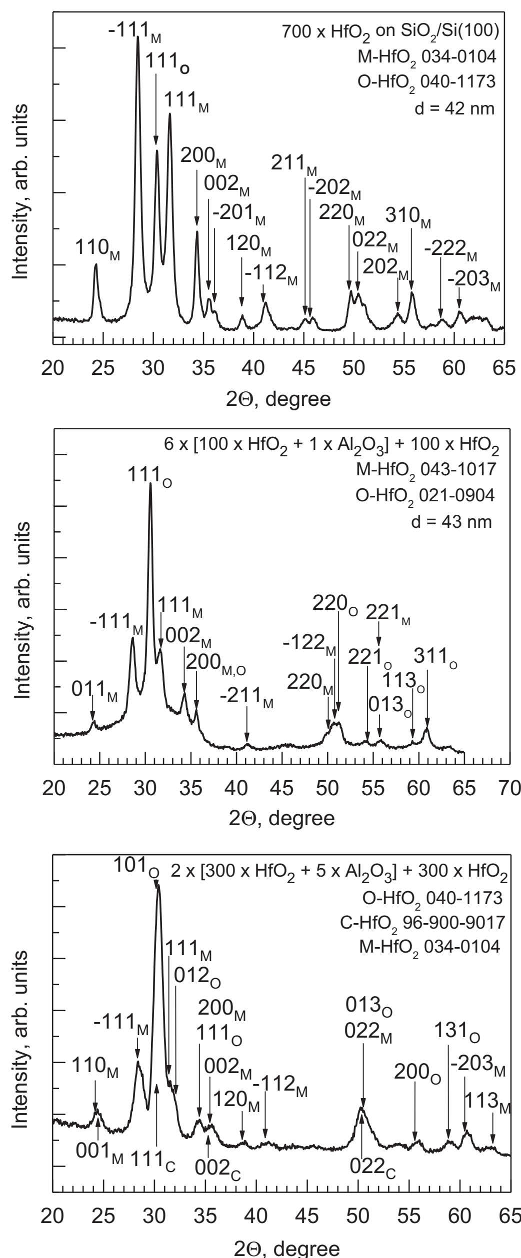

Figure 2. GIXRD patterns of reference HfO_2 film (top panel), a HfO_2:Al_2O_3 mixed with Al below the EDX detection level (middle panel), and a nanolaminate with Al_2O_3 Hf:Al cation ratio of 1.9 (bottom panel). The Miller indexes are supplied with subscripts M, O, and C, referring to the monoclinic, orthorhombic and cubic polymorphs of HfO_2, respectively. The arrows at indexes indicate the corresponding peak locations in accord with the reference powder diffraction files. The powder diffraction file numbers and film growth cycle sequences are indicated by labels.

Nanolaminate films built up on thin HfO_2 films separated by amorphous intermediate layers, such as Al_2O_3 in this study, demonstrate mixed crystal structures with strong contribution from both metastable and stable HfO_2 polymorphs. We have earlier observed that in HfO_2-Ta_2O_5 nanolaminates, where 2–20 nm thick HfO_2 intermediate layers were also grown in $HfCl_4$-based ALD process, the monoclinic phase started to form in addition to the cubic/tetragonal phases in quite early stages of growth, i.e. after the HfO_2 layer thickness exceeded 5 nm.[40]

In the HfO_2-Al_2O_3 nanolaminates with somewhat thinner HfO_2 layers of ca. 7 nm (Figure 3), separated by ca. 1 nm Al_2O_3 layers,

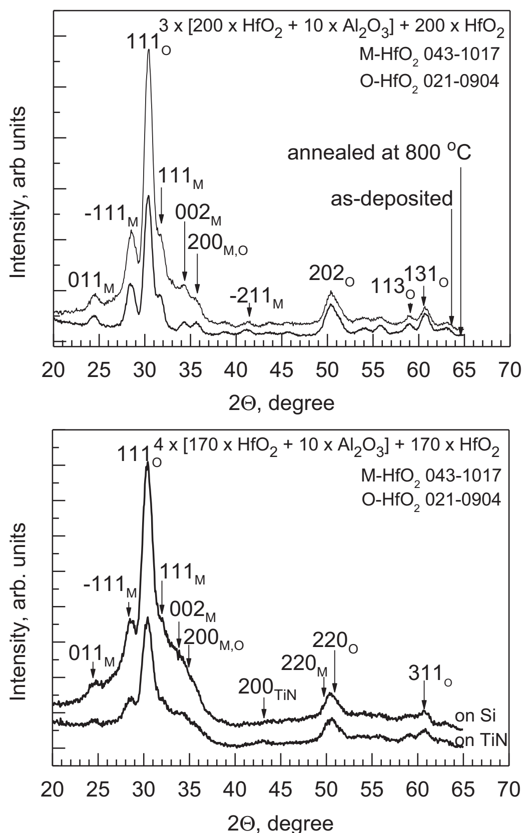

Figure 3. GIXRD patterns from HfO_2-Al_2O_3 nanolaminates with HfO_2 layers grown to nominal thicknesses of 10 nm (upper panel) and 8 nm (lower panel) alternately with ca. 0.5 nm thick Al_2O_3 layers. For comparison, patterns from the same films on Si and after annealing at 800°C (upper panel), and as-deposited on TiN substrate surface (lower panel) are presented. The Miller indexes are supplied with subscripts M and O, referring to the monoclinic and orthorhombic polymorphs of HfO_2, respectively. The arrows at indexes indicate the corresponding peak locations in accord with the reference powder diffraction files. The powder diffraction file numbers and film growth cycle sequences are indicated by labels.

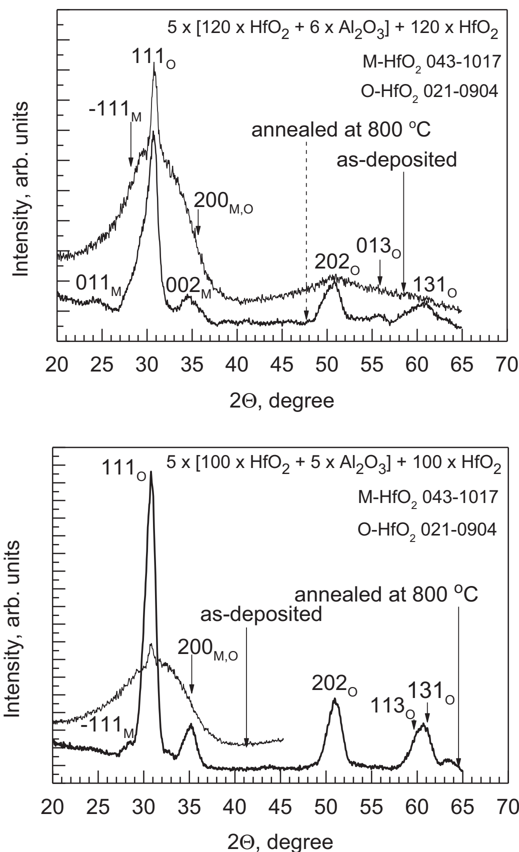

Figure 4. GIXRD patterns from HfO_2-Al_2O_3 nanolaminates with HfO_2 layers grown to nominal thicknesses of ca. 6 nm (upper panel) and 5 nm (lower panel) alternately with ca. 0.3 and 0.25 nm thick Al_2O_3 layers. Patterns from the same films as-deposited on Si and after annealing at 800°C are presented. The Miller indexes are supplied with subscripts M and O, referring to the monoclinic and orthorhombic polymorphs of HfO_2, respectively. The arrows at indexes indicate the corresponding peak locations in accord with the reference powder diffraction files. The file numbers and film growth cycle sequences are indicated by labels.

a metastable HfO_2 polymorph with reflections designated to the orthorhombic lattice appeared dominating over the monoclinic phase. One could also see that post-deposition annealing as well as the growth of the films on nanocrystalline 10 nm thick TiN layer did not induce qualitative changes in the phase composition of the oxide films (Figure 3). These films were thus notably resistant against phase changes upon annealing.

In the HfO_2-Al_2O_3 nanolaminates with HfO_2 and Al_2O_3 layers both grown to even lower thicknesses, nominally 5–6 nm and 0.23–0.30 nm, respectively, the metastable phases were dominant at least in the as-deposited state (Figure 4). Also notable was the amorphous background in the GIXRD patterns. Quite aggressive annealing at 800°C in air ambient for half an hour reduced the amorphous background significantly and increased the degree of crystallinity of the films, decided on the basis of the intensity and number of the diffraction peaks (Figure 4). Also the contribution from the monoclinic polymorph became apparent upon annealing.

Electrical and magnetic performance.—Selected films with the largest contribution from the metastable HfO_2 phases were subjected to electrical measurements. The relative permittivity of the films tended to increase with the HfO_2:Al_2O_3 cycle ratio. The relative permittivity, measured at 100 kHz, was increased from 14 to 22 (Table II) with the increase of Hf:Al cation ratio from 4.2 to 6.4. In the film containing aluminum below the EDX detection level, i.e. in the sample grown with the HfO_2:Al_2O_3 cycle ratio of 100:1, the permittivity was measured somewhat lower again, not exceeding 18. In the latter film, the contribution from monoclinic phase of HfO_2 was also increased compared to the samples with lower Hf:Al ratio and Al content measurable by EDX. One can see, that in the present series of films, the permittivity was somewhat correlated to the phase composition, increasing with the content of metastable phases expressed by the increasing intensity of the corresponding peaks in the XRD patterns, as was described above.

Somewhat surprisingly, the permittivity dispersion in the film grown with the HfO_2:Al_2O_3 cycle ratio of 170:10 was exeptionally strong (not shown), allowing one to measure relative permittivies above 60 in the frequency range of 1–10 kHz, probably due to the presence of strong dipolar and interfacial polarization mechanisms. The apparently high permittivity and dispersion might arise from the strongly polycrystalline and mixed phase nature of this film. For the rest of the samples, the dispersion at low frequencies was essentially weaker, demonstrating only 10% increase in the permittivity toward measurement frequencies down to 1 kHz. These low-frequency permittivies are quite close to those reported in our earlier studies on HfO_2 films grown by ALD in the temperature range of 300–400°C from $HfCl_4$ and H_2O.[35,40] Certain increase in the permittivities compared to the earlier published results is likely connected to the increased amount of metastable hafnium oxide phases in the films grown in the present study. Cubic and tetragonal phases of HfO_2 are known to

Table II. HfO_2:Al_2O_3 cycle ratio, Hf:Al cation ratio and permittivity, measured for selected repesentative films, in the ascending order for Hf content. Also indicated are the estimated values for the half-width of charge-field loops, designated as coercive field, and the charge density at zero field value, assigned as remnant polarization. The latter values are calculated for the charge-voltage loops, measured in the medium voltage range of −1 to 1 V, approximately, as depicted in Fig. 6.

HfO_2:Al_2O_3 cycle ratio	Hf:Al cation ratio	Relative permittivity	Coercive field, MV/cm	Remnant polarization, mC/cm^2
(100:5)	4.2	14.0	0.23	8.3
(120:6)	4.5	15.8	0.18	9.2
(200:10)	5.4	22.0	0.20	2.3
(170:10)	6.4	22.0	0.25	12.5
(100:1)	Al not measurable	18.0	0.28	3.7

possess higher permittivities than the stable monoclinic polymorph. Orientationally averaged static dielectric constants of 29, 70, and 16–18 have been obtained for the cubic, tetragonal, and monoclinic HfO_2 phases, respectively.[21]

Figure 5 demonstrates current-voltage behavior measured in resistive switching regime from the HfO_2-Al_2O_3 nanolaminate grown using the HfO_2:Al_2O_3 cycle ratio of 200:10. One can see that the films demonstrate current-voltage behavior similar to those studied as potential memristor materials. At both positive and negative bias voltages marked differences between the low and high resistance states were achieved, with a window ranging over almost an order of magnitude in the conduction current. The forming voltages, necessary to achieve the first highly conductive state in the material, varied between 1 and 2 V, which is still reasonably low voltage range considering the thickness of the films, exceeding 20 nm.

Figure 6 depicts the charge polarization– voltage loops measured by means of the Sawyer-Tower circuit from selected samples, in most of which the metastable HfO_2 phase or phases were dominating in accord with the GIXRD results. In these loops, one can recognize features characteristic of ferroelectric materials – the charge in the material may be drawn to saturation at the highest external voltages applied in both polarity directions. After sweeping the voltage back toward zero, remnant polarization charge can be recorded at zero bias voltage and hysteresis with marked coercive force develops in the back-forth swept curves. For comparison, in the ALD-grown noncentrosymmetric orthorhombic phase of HfO_2 stabilized by doping with foreign cations, well-defined ferroelectric hysteresis has been recorded.[23–25] In another study,[41] Al-doped HfO_2 films containing the cubic and/or orthorhombic polymorphs in addition to the monoclinic phase were grown by ALD at 300°C from $HfCl_4$, $Al(CH_3)_3$ and H_2O. In the latter films, ferroelectric behavior was recognized whereas the reliability of the capacitors was somewhat degraded by chemical changes at the oxide-TiN electrode interfaces. In the charge-voltage loops obtained in the present study, ferroelectric polarization component is, possibly, present, but the curves do not entirely match with the behavior of truly ferroelectric material, especially those measured under the widest ranges of voltages. At voltages comparable to those able to initiate formation of leaky channels and low resistive states in the oxide layer, marked contribution from the interfacial polarization due to considerable leakage currents should be taken into account. The charge polarizing these films and laminates deposited is at least partially due to carriers drifted from an electrode to the another one. The interfacial charge, though, may have partially been trapped at multiple barriers between the constituent metal oxide layers as well as at the interfaces between the metal oxide layers and Ti or TiN electrodes. The effect of the leakage distorting the charge-voltage behavior seems to strenghten somewhat upon the increment of the relative hafnium oxide content in the films. The leakage may also increase with the significance of the monoclinic phase of HfO_2 which makes the phase composition in the layer more heterogeneous.

Figure 7 depicts magnetization-field loops of HfO_2-Al_2O_3 nanolaminates recorded using a vibrating sample magnetometer. The magnetization in these ca. 40–50 nm thick films was strongly nonlinear and rapidly increased with the external field strength until 2000 Oe, approximately. The magnetization saturates upon further increment of the field and also exhibits certain coercivity along with sweeping the field strength and direction. The magnetization behavior thus resembles soft ferromagnetic materials.

The coercive field was somewhat larger at low measurement temperatures, reaching 400 Oe at 2 K in the film with a Hf:Al ratio of 5.4, i.e. in the nanolaminate structure grown with the HfO_2:Al_2O_3 pulse ratio of 200:10 (Table I) and possessing a structure of dominantly metastable HfO_2 polymorph (Fig. 3, upper panel). Within the composition and structure range of HfO_2:Al_2O_3 films explored in this study, the saturative behavior of both charge and magnetic polarization in external electric and magnetic fields was most clearly recognized in the film grown with the cycle ratio of 200:10.

Nonlinear saturative magnetization characteristic of ferromagnetic materials has been achieved and observed in un-doped HfO_2 films in some works earlier, such as in 10–200 nm thick HfO_2 films grown by pulsed laser deposition[42–44] and sputtering.[45] Magnetization in crystallized HfO_2 films has thereby been explained by presence of oxygen vacancies,[42–45] and the magnetization indeed could be suppressed by annealing in oxygen environment, i.e. upon improvement of the stoichiometry of the dioxide.[42,45] Magnetization in HfO_2 films has been similar to that in soft ferromagnetic materials with narrow hysteresis, which was observed also in the present study.

The residual impurities in the films can affect their physical properties, in general. In terms of electrical performance, the existence of measurable content of residual chlorine may, quite likely, increase the conductivity of the films and, thus, also the role of interfacial polarization contributing to the polarization charge and the remnant polarization as recorded at zero sample voltage. At the same time, the existence of residuals can assist in the stabilization of artificially defective structure, up to the partial formation of metastable hafnium oxide phases, and, in this way, give rise to magnetization of the solid films.

In ALD processes using metal halide and water precursors, the amounts of residual impurities decrease rapidly and nonlinearly with the increase in the growth temperature in the range of 200–600°C. In regard with the ALD process based on the $HfCl_4$ and H_2O precursors, ion beam analysis has shown residue contents in the ranges of 0.1–0.6 and 0.5–2.3 at.% for chlorine and hydrogen respectively, in films deposited at 300°C.[35] In the present study, the amount of residual chlorine in the films grown at 350°C remained, quite expectedly, lower than the limit for its reliable detection by EDX.

Summary

HfO_2-Al_2O_3 films and nanolaminates were grown by atomic layer deposition from hafnium tetrachloride, aluminum trichloride and water on silicon and titanium nitride substrates. The main goal of the work was to study the feasibility of the stabilization of the metastable polymorphs in HfO_2 by alternate layering of crystalline HfO_2 and amorphous Al_2O_3. The HfO_2:Al_2O_3 ALD cycle ratio was varied between 200:10 and 15:1 in order to grow of multilayers consisting of distinct binary oxides or mixtures and, by this way, tune the phase composition of the resulting films. The contribution of the metastable cubic and, possibly, orthorhombic HfO_2 polymorphs increased with the relative content and thickness of aluminum oxide layers, while the intensity of the crystal growth in the HfO_2 layers increased with their thickness.

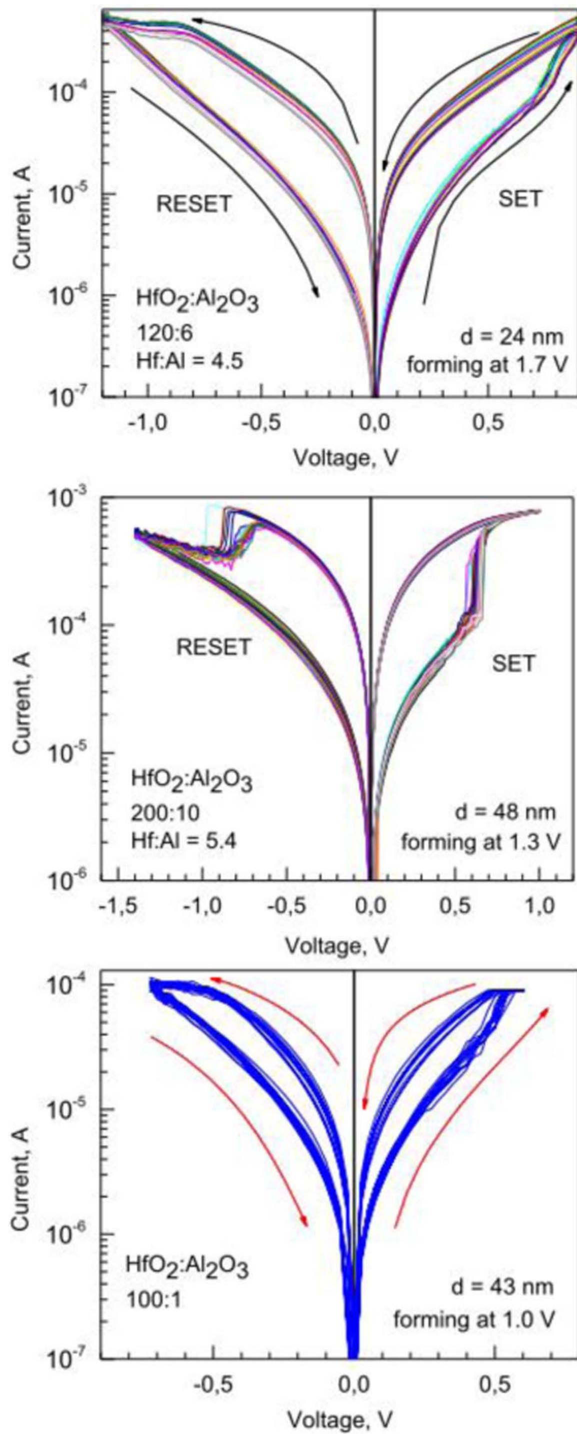

Figure 5. Current-voltage loops measured in resistive switching regime from selected HfO_2-Al_2O_3 nanolaminate films described by labels and Table I. HfO_2:Al_2O_3 growth cycle ratios, film thicknesses, d, and electroforming voltage values are indicated by labels.

The films exhibited polarization charge-electric field loops, affected by interfacial polarization. Two distinctive resistance states were observed in the current-voltage loops of the nanolaminate films as characteristic of resistive switching memory materials. The films could also be saturatively magnetized and they exhibited soft ferromagnetic behavior with weak coercive field in the magnetization-field hystereses. The magnetoelectric properties were recognized at room temperature and most clearly in the well-defined nanolaminate film

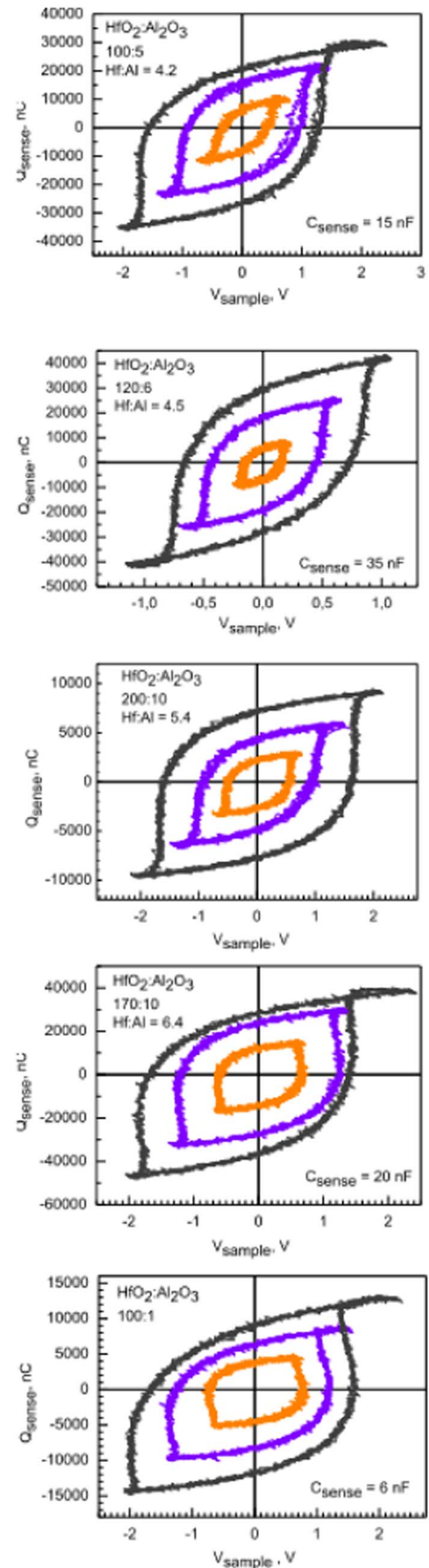

Figure 6. Charge on sense capacitor versus voltage applied on Al/Ti//HfO_2-Al_2O_3/TiN/Si/Al structures as sample capacitors in series with sense capacitors in Sawyer-Tower circuits. Film growth cycle sequences, thicknesses, and sense capacitances used are given by labels. Different colors denote the measurements in variable sample voltage ranges.

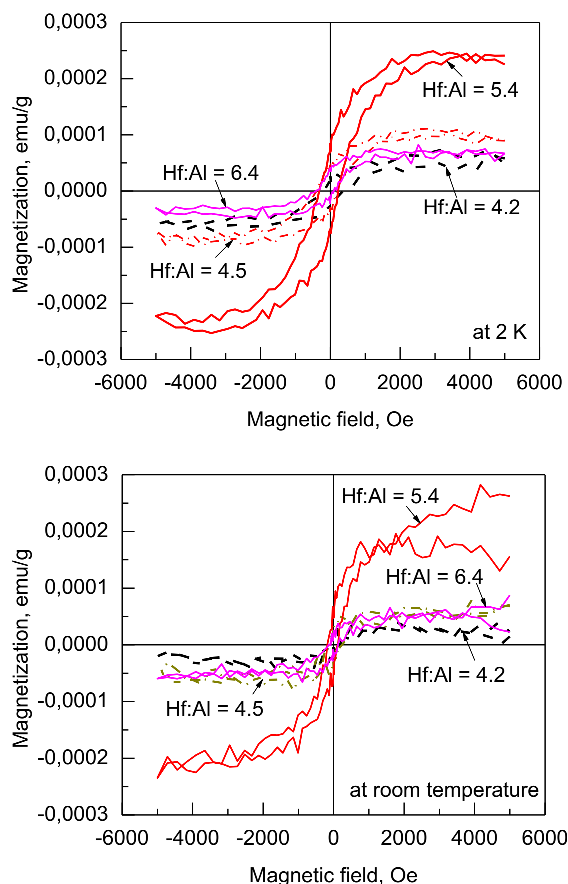

Figure 7. Magnetization in HfO_2-Al_2O_3 films against external magnetic field strength at 2 K (upper panel) and room temperature (lower panel). The Hf:Al cation ratios measured by EDX are given by labels. For detailed sample description, see Table I.

grown with the HfO_2:Al_2O_3 cycle ratio of 200:10. In this nanolaminate, the metastable polymorphs of HfO_2 dominated the phase composition.

Acknowledgments

The study was partially supported by the Finnish Centre of Excellence in Atomic Layer Deposition (284623), European Regional Development Fund project "Emerging orders in quantum and nanomaterials" (TK134), Spanish Ministry of Economy and Competitiveness (TEC2014-52152-C3-3-R) with support of Feder fund, Estonian Research Agency (IUT2-24, IUT23-7, PRG4), and Estonian Academy of Sciences (SLTFYPROF).

ORCID

Kaupo Kukli https://orcid.org/0000-0002-5821-0364
Marianna Kemell https://orcid.org/0000-0002-3583-2064
Helena Castán https://orcid.org/0000-0002-3874-721X
Salvador Dueñas https://orcid.org/0000-0002-2328-1752
Helina Seemen https://orcid.org/0000-0002-4850-0851
Raivo Stern https://orcid.org/0000-0002-6724-9834
Mikko Ritala https://orcid.org/0000-0002-6210-2980

References

1. C. Martínez-Domingo, X. Saura, A. Conde, D. Jiménez, E. Miranda, J. M. Rafí, F. Campabadal, and J. Suñé, "Initial leakage current related to extrinsic breakdown in HfO_2/Al_2O_3 nanolaminate ALD dielectrics," *Microel. Eng.*, **88**, 1380 (2011).
2. M. Liu, G. He, L. Q. Zhu, Q. Fang, G. H. Li, and L. D. Zhang, "Microstructure and interfacial properties of HfO_2 –Al_2O_3 nanolaminate films," *Appl. Surf. Sci.*, **252**, 6206 (2006).
3. A. Gómez, H. Castán, H. García, S. Dueñas, L. Bailón, F. Campabadal, J. M. Rafí, and M. Zabala, "Electrical characterization of high-k based metal-insulator-semiconductor structures with negative resistance effect when using Al_2O_3 and nanolaminated films deposited on p-Si," *J. Vac. Sci. Technol. B*, **29**, 01A901 (2011).
4. F. Campabadal, J. M. Rafí, M. Zabala, O. Beldarrain, A. Faigón, H. Castán, A. Gómez, H. García, and S. Dueñas, "Electrical characteristics of metal-insulator-semiconductor structures with atomic layer deposited Al_2O_3, HfO_2, and nanolaminates on different silicon substrates," *J. Vac. Sci. Technol. B*, **29**, 01AA07 (2011).
5. D. Cao, X. Cheng, L. Zheng, D. Xu, Z. Wang, C. Xia, L. Shen, Y. Yu, and D. Shen, "Low-temperature plasma-enhanced atomic layer deposition of HfO_2/Al_2O_3 nanolaminate structure on Si," *J. Vac. Sci. Technol. B*, **33**, 01A101 (2015).
6. S. Persson, D. Wu, P.-E. Hellström, S.-L. Zhang, and M Östling, "Quantifying hole mobility degradation in pMOSFETs with a strained-$Si_{0.7}Ge_{0.3}$ surface-channel under an ALD TiN/Al_2O_3/$HfAlO_x$/Al_2O_3 gate stack," *Solid-State Electr.* **48** 721 (2004).
7. C. Mahata, Y.-C. Byun, C.-H. An, S. Choi, Y. An, and H. Kim, "Comparative study of atomic-layer-deposited stacked (HfO_2/Al_2O_3) and nanolaminated ($HfAlO_x$) dielectrics on $In_{0.53}Ga_{0.47}As$," *ACS Appl. Mater. Interfaces*, **5**, 4195 (2015).
8. E. Cianci, A. Molle, A. Lamperti, C. Wiemer, S. Spiga, and M. Fanciulli, "Phase stabilization of Al:HfO_2 grown on $In_xGa_{1-x}As$ Substrates (x = 0, 0.15, 0.53) via trimethylaluminum-based atomic layer deposition," *ACS Appl. Mater. Interfaces*, **6**, 3455 (2014).
9. C.-H. An, C. Mahata, Y.-C. Byun, and H. Kim, "Atomic-layer-deposited $(HfO_2)_{1-x}(Al_2O_3)_x$ nanolaminate films on InP with different Al_2O_3 contents," *J. Phys. D: Appl. Phys.*, **46**, 275301 (2013).
10. C. Mahata, Y. An, S. Choi, Y.-C. Byun, D.-K. Kim, T. Lee, J. Kim, M.-H. Cho, and H. Kim, "Electrical properties of the HfO_2-Al_2O_3 nanolaminates with homogeneous and graded compositions on InP," *Curr. Appl. Phys.*, **16**, 294 (2016).
11. S.-G. Kim, C.-S. Hyun, D. Park, T.-H. Cho, J.-G. Suk, H.-S. Hong, K.-Y. Lee, and K.-S. Oh, "Fully integrated 512 Mb DRAMs with HSG-merged-AHO cylinder capacitor," *Solid State Electr.* **50**, 1030 (2006).
12. H.-Y. Gou, S. Chen, S.-J. Ding, Q.-Q. Sun, H.-L. Lu, D. W. Zhang, and P.-F. Wang, "Influence of HfAlO composition on memory effects of metal-oxide-semiconductor capacitors with Al_2O_3 /HfAlO/Al_2O_3 layers and Pd electrode," *Thin Solid Films*, **529**, 380 (2012).
13. S. Sakai and M. Takahashi, "Recent progress of ferroelectric-gate field-effect transistors and applications to nonvolatile logic and FeNAND flash memory," *Materials*, **3**, 4950 (2010).
14. L.-G. Wang, X. Qian, Y.-Q. Cao, Z.-Y. Cao, G.-Y. Fang, A.-D. Li, and D. Wu, "Excellent resistive switching properties of atomic layer-deposited $Al_2O_3/HfO_2/Al_2O_3$ trilayer structures for non-volatile memory applications," *Nanoscale Res. Lett.*, **10**, 135 (2015).
15. M. Bonvalot, M. Kahn, C. Vallée, E. Gourvest, H. Abed, C. Jorel, and C. Dubourdieu, "Combined spectroscopic ellipsometry and attenuated total reflection analyses of Al_2O_3/HfO_2 nanolaminates," *Thin Solid Films*, **518**, 5057 (2010).
16. A. Markeev, A. Chouprik, K. Egorov, Yu. Lebedinskii, A. Zenkevich, and O. Orlov, "Multilevel resistive switching in ternary $Hf_xAl_{1-x}O_y$ oxide with graded Al depth profile," *Microel. Eng.*, **109**, 342 (2013).
17. E. Covi, S. Brivio, M. Fanciulli, and S. Spiga, "Synaptic potentiation and depression in Al:HfO_2-based memristor," *Microel. Eng.*, **147**, 41 (2015).
18. J. Frascaroli, F. G. Volpe, S. Brivio, and S. Spiga, "Effect of Al doping on the retention behavior of HfO_2 resistive switching memories," *Microel. Eng.*, **147**, 104 (2015).
19. A. Paskaleva, M. Rommel, A. Hutzler, D. Spassov, and A. J. Bauer, "Tailoring the electrical properties of HfO_2 MOS-Devices by aluminum doping" *ACS Appl. Mater. Interfaces*, **7**, 17032 (2015).
20. T. J. Park, J. H. Kim, J. H. Jang, C.-K. Lee, K. D. Na, S. Y. Lee, H.-S. Jung, M. Kim, S. Han, and C. S. Hwang, " Reduction of electrical defects in atomic layer deposited HfO_2 films by Al Doping" *Chem. Mater.*, **22**, 4175 (2010).
21. X. Zhao and D. Vanderbilt, "First-principles study of structural, vibrational, and lattice dielectric properties of hafnium oxide," *Phys. Rev. B*, **65**, 233106 (2002).
22. J. Robertson and R. M. Wallace, "High-K materials and metal gates for CMOS applications," *Mater. Sci. Eng. R*, **88**, 1 (2015).
23. J. Müller, T. S. Böscke, S. Müller, E. Yurchuk, P. Polakowski, J. Paul, D. Martin, T. Schenk, K. Khullar, A. Kersch, W. Weinreich, S. Riedel, K. Seidel, A. Kumar, T. M. Arruda, S. V. Kalinin, T. Schlösser, R. Boschke, R. van Bentum, U. Schröder, and T. Mikolajick, "Ferroelectric hafnium oxide: A CMOS-compatible and highly scalable approach to future ferroelectric memories," *IEEE Int. Electr. Dev. Meeting*, 10.8.1. (2013).
24. J. Müller, P. Polakowski, S. Mueller, and T. Mikolajick, "Ferroelectric hafnium oxide based materials and devices: Assessment of current status and future prospects," *ECS J. Solid State Sci. Tech.*, **4**, N30 (2015).
25. M. H. Park, T. Schenk, C. M. Fancher, E. D. Grimley, C. Zhou, C. Richter, J. M. LeBeau, J. L. Jones, T. Mikolajick, and U. Schroeder, "A comprehensive study on the structural evolution of HfO_2 thin films doped with various dopants," *J. Mater. Chem. C*, **5**, 4677, (2017).
26. S. Mueller, J. Mueller, A. Singh, S. Riedel, J. Sundqvist, U. Schroeder, and T. Mikolajick, "Incipient ferroelectricity in Al-doped HfO_2 thin films," *Adv. Funct. Mater.*, **22**, 2412 (2012).
27. K. Kalantar-zadeh, J. Z. Ou, T. Daeneke, A. Mitchell, T. Sasaki, and M. S. Fuhrer, "Two dimensional and layered transition metal oxides," *Appl. Mater. Today*, **5**, 73, (2016).

28. M.-C. Kao, H.-Z. Chen, S.-L. Young, K.-H. Chen, J.-L. Chiang, and J.-B. Shi, Structural, electrical, magnetic and resistive switching properties of the multiferroic/ferroelectric bilayer thin films, *Materials*, **10**, 1327 (2017).
29. S. Ren, G. Zhu, J. Xie, J. Bu, H. Qin, and J. Hu, "Resistive switching and electrical control of ferromagnetism in a Ag/HfO_2/Nb:$SrTiO_3$/Ag resistive random access memory (RRAM) device at room temperature," *J. Phys.: Cond. Mat.*, **28**, 056001 (2016).
30. S. Ren, H. Qin, J. Bu, G. Zhu, J. Xie, and J. Hu, "Coexistence of electric field controlled ferromagnetism and resistive switching for TiO_2 film at room temperature," *Appl. Phys. Lett.*, **107**, 062404 (2015).
31. A. Chouprik, A. Chernikova, A. Markeev, V. Mikheev, D. Negrov, M. Spiridonov, S. Zarubin, and A. Zenkevich, "Electron transport across ultrathin ferroelectric $Hf_{0.5}Zr_{0.5}O_2$ films on Si," *Microel. Eng.*, **178**, 250 (2017).
32. K. Kukli, M. Kemell, H Castán, S. Dueñas, H. Seemen, M. Rähn, J. Link, R. Stern, M. J. Heikkilä, M. Ritala, and M. Leskelä, "Atomic layer deposition and performance of ZrO_2-Al_2O_3 thin films," *ECS J. Solid State Sci. Tech.*, **7**, P287 (2018).
33. T. Wang and J. G. Ekerdt, "Structure versus thermal stability: The periodic structure of atomic layer deposition-grown Al-incorporated HfO_2 films and its effects on amorphous stabilization", *Chem. Mater.*, **23**, 1679 (2011).
34. R. Lo Nigro, E. Schilirò, G. Greco, P. Fiorenza, and F. Roccaforte, "Laminated Al_2O_3–HfO_2 layers grown by atomic layer deposition for microelectronics applications," *Thin Solid Films*, **601**, 68 (2016).
35. K. Kukli, J. Aarik, M. Ritala, T. Uustare, T. Sajavaara, J. Lu, J. Sundqvist, A. Aidla, L. Pung, A. Hårsta, and M. Leskelä, "Effect of selected atomic layer deposition parameters on the structure and dielectric properties of hafnium oxide films," *J. Appl. Phys.*, **96**, 5398 (2004).
36. K. Kukli, J. Aarik, T. Uustare, J. Lu, M. Ritala, A. Aidla, L. Pung, A. Hårsta, M. Leskelä, A. Kikas, and V. Sammelselg, "Engineering structure and properties of hafnium oxide films by atomic layer deposition temperature," *Thin Solid Films*, **479**, 1 (2005).
37. T. Suntola, "Atomic layer epitaxy," *Thin Solid Films*, **216**, 84 (1992).
38. R. A. Waldo, *Microbeam Analysis*, (San Francisco Press, San Francisco, CA, 1988), p. 310.
39. K. Kukli, M. Kemell, H. Castán, S. Dueñas, H. Seemen, M. Rähn, J. Link, R. Stern, M. J. Heikkilä, M. Ritala, and M. Leskelä, "Atomic layer deposition and performance of ZrO_2-Al_2O_3 thin films," *ECS J. Solid State Sci. Technol.*, **7**, P287 (2018).
40. K. Kukli, J. Ihanus, M. Ritala, and M. Leskelä, "Tailoring the dielectric properties of HfO_2–Ta_2O_5 nanolaminates," *Appl. Phys. Lett.*, **68**, 3737 (1996).
41. K. Florent, S. Lavizzari, M. Popovici, L. Di Piazza, U. Celano, G. Groeseneken, and J. Van Houdt, "Understanding ferroelectric Al:HfO_2 thin films with Si-based electrodes for 3D applications," *J. Appl. Phys.*, **121**, 204103 (2017).
42. N. H. Hong, "Magnetism due to defects/oxygen vacancies in HfO_2 thin films," *Phys. Stat. Sol.*, **4**, 1270 (2007).
43. O. E. Tereshchenko, V. A. Golyashov, S. V. Eremeev, I. Maurin, A. V. Bakulin, S. E. Kulkova, M. S. Aksenov, V. V. Preobrazhenskii, M. A. Putyato, B. R. Semyagin, D. V. Dmitriev, A. I. Toropov, A. K. Gutakovskii, S. E. Khandarkhaeva, I. P. Prosvirin, A. V. Kalinkin, V. I. Bukhtiyarov, and A. V. Latyshev, "Ferromagnetic HfO_2/Si/GaAs interface for spin-polarimetry applications," *Appl. Phys. Lett.*, **107**, 123506 (2015).
44. K. K. Bharathi, S. Venkatesh, G. Prathiba, N. H. Kumar, and C. V. Ramana, "Room temperature ferromagnetism in HfO_2 films," *J. Appl. Phys*.**109**, 07C318 (2011).
45. J. M. D. Coey, M. Venkatesan, P. Stamenov, C. B. Fitzgerald, and L. S. Dorneles, "Magnetism in hafnium dioxide," *Phys. Rev. B*, **72**, 024450 (2005).